A Multi-DOF Soft Robot Mechanism for Patient Motion Correction and Beam Orientation Selection in Cancer Radiation Therapy.

Lekan Ogunmolu

Department of Electrical Engineering

The University of Texas at Dallas, Richardson, TX

May 16, 2019

Publications

- **Olalekan Ogunmolu**, A Multi-DOF Soft Robot Mechanism for Patient Motion Correction and Beam Orientation Selection in Cancer Radiation Therapy. PhD Thesis Manuscript. Hyperlink: utdallas.edu/ opo140030/media/Papers/thesis.pdf
- Azar Sadeghnejad Barkousaraie, **Olalekan Ogunmolu**, Steve Jiang, and Dan Nguyen. A Fast Deep Learning Approach for Beam Orientation Selection Using Supervised Learning with Column Generation on IMRT Prostate Cancer Patients. Under review at *Medical Physics* (Journal), April 2019.
- **Olalekan Ogunmolu**, Michael Folkerts, Dan Nguyen, Nicholas Gans, and Steve Jiang. Deep BOO! Automating Beam Orientation Selection in Intensity Modulated Radiation Therapy. *Algorithmic Foundations of Robotics XIII, International Workshop* (*WAFR*), Mérida, Mexico. December 2018. Published in Springer's Proceedings in Advanced Robotics (SPAR) Book. 2019.
- **Olalekan Ogunmolu**, Nicholas Gans, Tyler Summers. Minimax Iterative Dynamic Game: Application to Nonlinear Robot Control Tasks. *IEEE/RSJ International Conference on Intelligent Robots and Systems* (*IROS*), Madrid, Spain. October 2018.
- **Olalekan Ogunmolu**, Adwait Kulkarn, Yonas Tadesse, Xuejun Gu, Steve Jiang, and Nicholas Gans. Soft-NeuroAdapt: A 3-DOF Neuro-Adaptive Pose Correction System For Frameless and Maskless Cancer Radiotherapy. *IEEE/RSJ International Conference on Intelligent Robots and Systems* (*IROS*), Vancouver, BC, Canada. September 2017. DOI: 10.1109/IROS.2017.8206211.
- Azar Sadeghnejad Barkousaraie, **Olalekan Ogunmolu**, Steve Jiang, and Dan Nguyen. Using supervised learning and guided Monte Carlo tree search for beam orientation optimization in radiation therapy. Under review at *International Conference on Medical Image Computing and Computer Assisted Intervention, XXII* (*MICCAI*), Shenzhen, China. October 2019.

Publications

- Azar Sadeghnejad Barkousaraie, **Olalekan Ogunmolu**, Steve Jiang, and Dan Nguyen. Deep Learning Neural Network for Beam Orientation Optimization. To appear in *International Conference on the use of Computers in Radiation Therapy XVI* (*ICCR*), Montreal, CA. June 2019.

- **Olalekan Ogunmolu**, Dan Nguyen, Xun Jia, Weiguo Lu, Nicholas Gans, and Steve Jiang. Automating Beam Orientation Optimization for IMRT Treatment Planning: A Deep Reinforcement Learning Approach. Selected for Oral Presentation at the *John R. Cameron Young Investigators Symposium – 60th Annual Meeting of the American Association of Physicists in Medicine*, Nashville, TN (*AAPM*). July 2018.

- Yara Almubarak, Joshi Aniket, **Olalekan Ogunmolu**, Xuejun Gu, Steve Jiang, Nicholas Gans, and Yonas Tadesse, Design and Development of Soft Robots for Head and Neck Cancer Radiotherapy. *SPIE: Smart Structures + Nondestructive Evaluation*, (*SPIE*), Denver, CO, U.S.A. March 2018.

- **Olalekan Ogunmolu**, Xuejun Gu, Steve Jiang, and Nicholas Gans. Vision-based control of a soft-robot for Maskless Cancer Radiotherapy. *IEEE Conference on Automation Science and Engineering (CASE)*, Fort-Worth, Texas, August 2016. DOI: 10.1109/CoASE.2016.7743378.

- **Olalekan Ogunmolu**, Xuejun Gu, Steve Jiang, and Nicholas Gans. A Real-Time Soft-Robotic Patient Positioning System for Maskless Head-and-Neck Cancer Radiotherapy. *IEEE Conference on Automation Science and Engineering (CASE)*, Gothenburg, Sweden, August 2015. DOI: 10.1109/CoASE.2015.7294318.

Three Dimensional Conformal Radiation Therapy

- Intensity Modulation: Control external beam's physical delivery
- *Conform* internally uniform fields with MLCs using a projection of target volumes [Boyer et al. (1992)]
- Improve tumor's local control

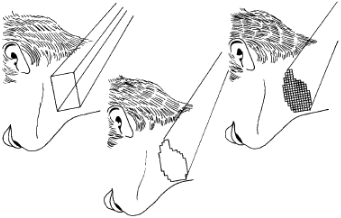

L-R: Conventional radiotherapy. Conformal radiotherapy (CFRT) without intensity modulation. CFRT with intensity modulation. Reprinted from Webb (2001).

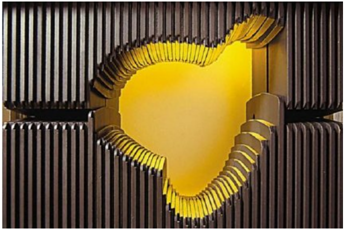

A multi-leaf collimator for IMRT/3DCRT. ©Varian Medical Systems.

Conformal RT Treatment Planning Parameters

- Optimal treatment *parameters* ▷ good treatment outcome
  - dose-limiting structures
  - OARs within a target volume
  - doctor's dose prescription
  - dose fractionation
  - **patient positioning**
  - **dose distribution**

Frame-based Radiotherapy Treatment

- Accurately irradiate a *moving target* and a *moving patient* with the aid of robots[Schweikard et al. (1995); Webb (1999)]

Frameless and Maskless Radiotherapy

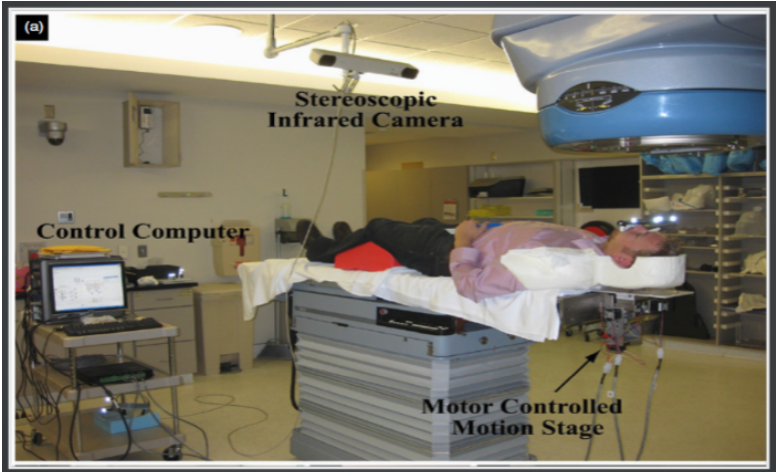

© Wiersma et al. (2009)

HexaPOD

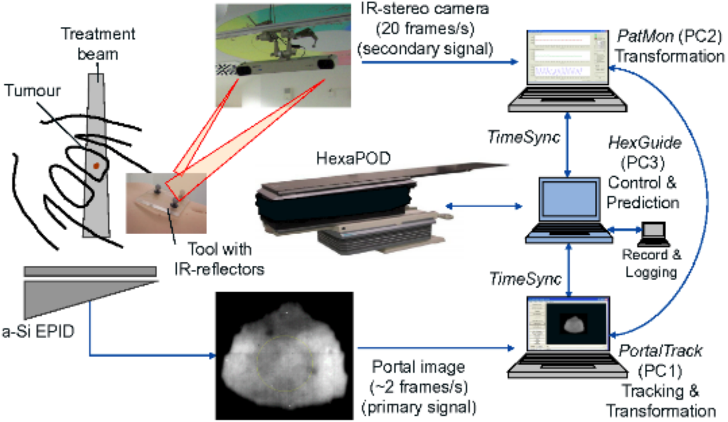

Reprinted from Herrmann et al. (2011)

Cyberknife/Novalis systems

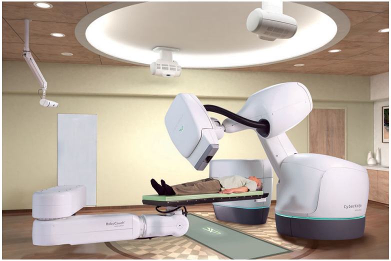

The Novalis ExacTrac Module

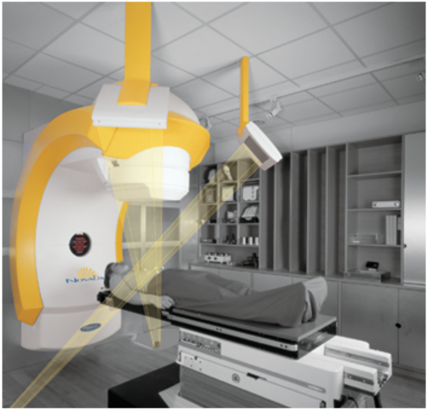

©Novalis

The Case for Soft Robots

- Frame-based immobilization
  - LINAC misalignments $\implies$ negative dosimetry effects
  - $\times$ Fractionated treatments
- Frameless RT
  - Incompatible with most conventional LINACs
- Cyberknife/Novalis Systems
  - Reliance on pre-treatment images
  - Rigid motion compensation issues
- Involuntary patient motion requires adaptive positioning

[0] Morphological computation, Cephalopods, Adaptive Controller for changing head dynamics: shape, weight etc

Beam Orientation Optimization

- During treatment planning, a **b**eam **o**rientation **o**ptimization problem (BOO) is separately solved
- Radiation is delivered from $\approx (5 - 15)$ different beam orientations during IMRT
- BOO determines the best beam angle combinations for delivering radiation
- Process of determining beamlets' intensities is termed **fluence map optimization** (FMO)

Vision-based 1-DOF Control

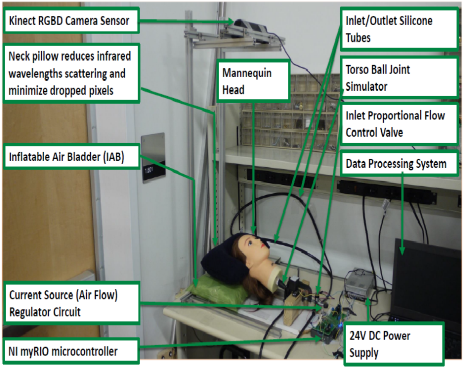

Sensors' Noise Floor

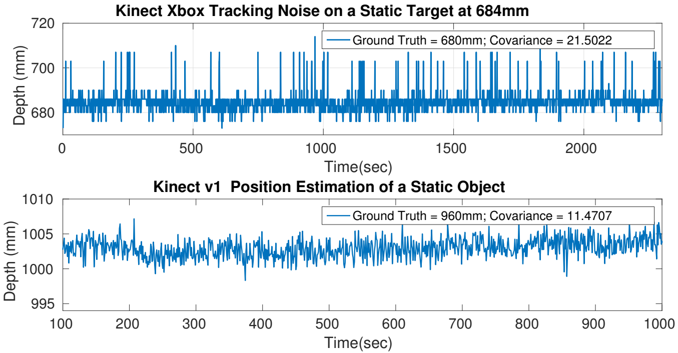

Kalman Filter Model

$$\begin{aligned}
\mathbf{x}(k) &= \mathbf{F}(k)\mathbf{x}(k-1) + \mathbf{B}(k)\mathbf{u}_k + \mathbf{G}_k\mathbf{w}_k \\
z_s &= \mathbf{H}_s(k)\mathbf{x}(k) + v_s(k) \qquad\qquad s = 1, 2 \\
\mathbf{F} &= \begin{bmatrix} 1 & \Delta T \\ 0 & 1 \end{bmatrix};\; a_k \sim \mathcal{N}(0, \sigma_a);\; \mathbf{G}_k = \mathbf{I}_{2x2}; \\
\mathbf{w}(k) &\sim \mathcal{N}(0, \mathbf{Q}(k)),\;\; \mathbf{W}(k) = \begin{pmatrix} \frac{\Delta T^2}{2} \\ \Delta T \end{pmatrix} \\
\mathbf{Q} &= \mathbf{W}\mathbf{W}^T {\sigma_a}^2 = \begin{bmatrix} \frac{\Delta T^4}{4} & \frac{\Delta T^3}{2} \\ \frac{\Delta T^3}{2} & \Delta T^2 \end{bmatrix} {\sigma_a}^2. \qquad (1)
\end{aligned}$$

State Estimates — Global Fusion of Local Tracks

- **Prediction:**

$$\begin{aligned} \hat{\mathbf{x}}_{k|k-1} &= \mathbf{F}\hat{\mathbf{x}}_{k-1|k-1} + \mathbf{B}_k \mathbf{u}_k \\ \mathbf{P}_{k|k-1} &= \mathbf{F}_k \mathbf{P}_{k-1|k-1} {\mathbf{F}_k}^T + \mathbf{Q}_k \end{aligned} \tag{2}$$

- **Update:**

$$\begin{aligned} \mathbf{K}(k) &= \mathbf{P}(k|k-1)\mathbf{H}(k)^T[\mathbf{H}(k)\mathbf{P}(k|k-1)\mathbf{H}(k)^T + \mathbf{R}(k)]^{-1} \\ \hat{\mathbf{x}}(k|k) &= \hat{\mathbf{x}}(k|k-1) + \mathbf{K}(k)(\mathbf{z}(k) - \mathbf{H}(k)\hat{\mathbf{x}}(k|k-1)) \\ \mathbf{P}(k|k) &= (\mathbf{I} - \mathbf{K}(k)\mathbf{H}(k))\mathbf{P}(k|k-1) \end{aligned} \tag{3}$$

Filtering Results

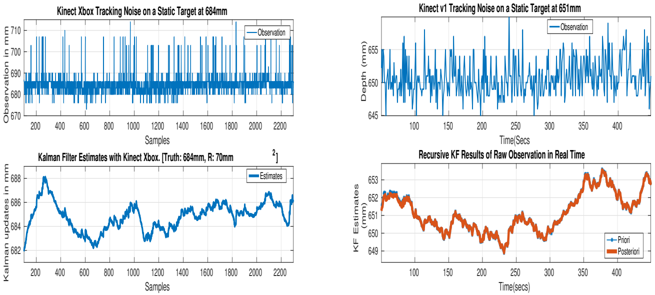

Xbox vs. Kinect v1

- **Fusion:**

$$\hat{\mathbf{x}}(F)(k|k) = \mathbf{P}(F)(k|k)\sum_{s=1}^{N}\left[\mathbf{P}(s)^{-1}(k|k)\hat{\mathbf{x}}(s)(k|k)\right]$$

Fusion Results

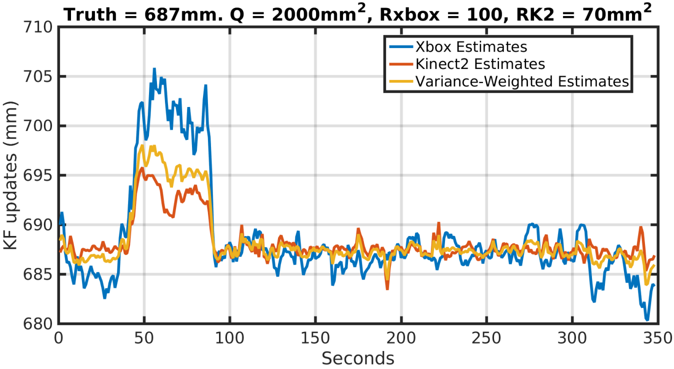

Fusion of local state estimates.

System Model and LQG Control

- Obtain optimal model parameters from I/O data through,

$$G(t) = \arg\min_{\theta} \; V_N(\theta, \phi_N) \tag{4}$$

- From (4), we obtained

$$\begin{aligned} \mathbf{x}(k+Ts) &= \mathbf{A}\mathbf{x}(k) + \mathbf{B}\mathbf{u}(k) + \mathbf{K}\mathbf{e}(k) \\ \mathbf{y}(k) &= \mathbf{C}\mathbf{x}(k) + \mathbf{D}\mathbf{u}(k) + \mathbf{e}(k) \end{aligned} \tag{5}$$

- LQG cost:

$$J = \sum_{k=0}^{\mathcal{K}} x^T(k)\, Q\, x(k) + u(k)^T\, R\, u(k) + 2x(k)^T\, N\, u(k)$$

- Find u from $\Delta u = \arg\min_{\Delta u} \; J$

1-DOF Control Results

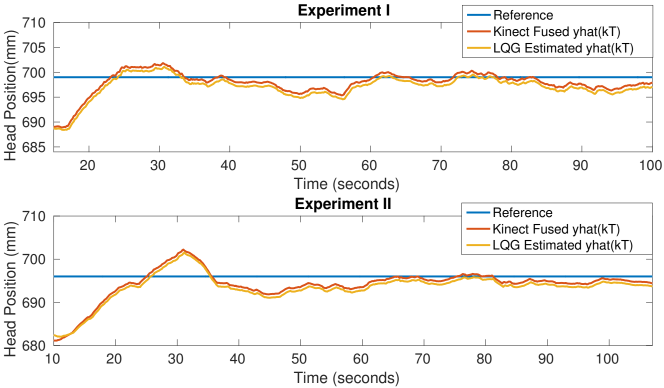

LQG Controller on mannequine head.

Vision-based 3-DOF Control

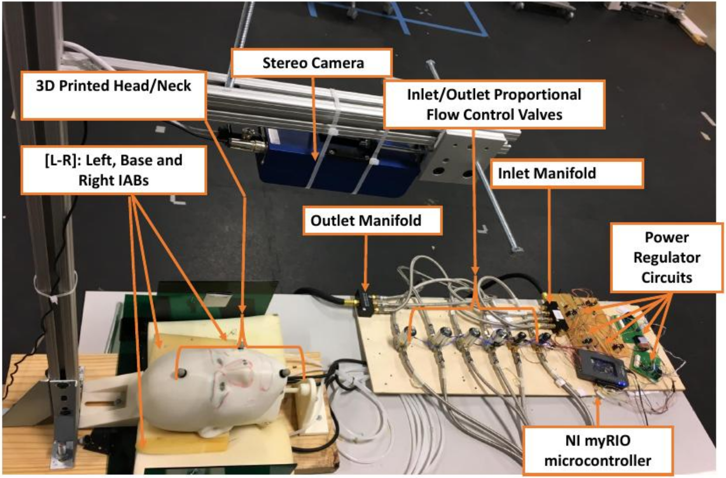

Hardware Description

Point Cloud Pre-Processing

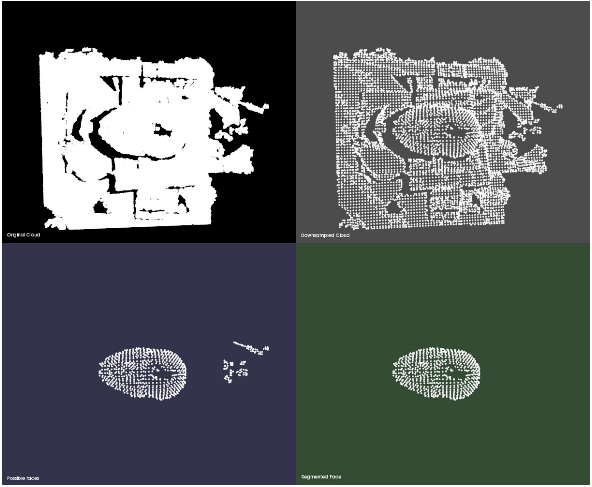

Head Pose Estimation

- Set cloud's centroid as measured point set $\mathbf{P} = \{\vec{p}_i\}$
- Get covariance matrix Σ_{px} of measured and model point sets: $\mathbf{P}$ and $\mathbf{X}$
- Set cyclic components of anti-symmetric matrix as Δ
- Set $\mathbf{Q}(\boldsymbol{\Sigma}_{px}) = \begin{bmatrix} \mathbf{tr}(\boldsymbol{\Sigma}_{px}) & \boldsymbol{\Delta}^T \\ \boldsymbol{\Delta} & \boldsymbol{\Sigma}_{px} + \boldsymbol{\Sigma}_{px}^T - \mathbf{tr}(\boldsymbol{\Sigma}_{px})\mathbf{I}_3 \end{bmatrix}$
- $q_R = \max_{\text{eig}}(\mathbf{Q}(\boldsymbol{\Sigma}_{px}))$; $q_T = \mu_x - \mathbf{R}(q_R)\mu_p$
- $x_h = (q_T, q_R)$

Model Reference Adaptive Control

- Head and IAB System Model

$$\dot{\mathbf{y}} = \mathbf{A}\mathbf{y} + \mathbf{B}\boldsymbol{\Lambda}\left(\mathbf{u} - f(\mathbf{y}, \mathbf{u})\right) + \mathbf{w}(k)$$

- Realize $f(\mathbf{y},\, \mathbf{u})$ with an RNN $\equiv \Theta^T \Phi(\mathbf{y})$
- In a ball $\mathbf{B}_R \subset D$
  - an ideal neural network (NN) approximation $f(\cdot) : \mathbb{R}^n \to \mathbb{R}^m$, can be realized to a sufficient degree of accuracy, $\varepsilon_f > 0$;
- Outside $\mathbf{B}_R$:
  - $\|\varepsilon(\mathbf{y})\| \leq k_{\max}(\mathbf{y}), \quad \forall \quad \mathbf{y} \in \mathbf{B}_R;$

Adaptive Neuro-Control Scheme

- Choose $\dot{\mathbf{y}}_m = \mathbf{A}_m y_m + \mathbf{B}_m \mathbf{r}$
- Knowns: B_m and an Hurwitz A_m
- $\mathbf{u} = \underbrace{\hat{\mathbf{K}}_y^{\mathbf{T}} \mathbf{y}}_{\text{state feedback}} + \underbrace{\hat{\mathbf{K}}_r^{\mathbf{T}} \mathbf{r}}_{\text{optimal regulator}} + \underbrace{\hat{f}(\mathbf{y}, \mathbf{u})}_{\text{approximator}}$
- $\hat{\mathbf{K}}_y$ and $\hat{\mathbf{K}}_r$ are adaptive gains to be designed. NB: $\tilde{\mathbf{K}}_x = \mathbf{K}_x - \hat{\mathbf{K}}_x$
- Assume ideal model matching conditions $\hat{\mathbf{K}}_y = \mathbf{K}_y$, and $\hat{\mathbf{K}}_r = \mathbf{K}_r$

Lyapunov Analysis

- **Theorem:** Given correct choice of adaptive gains $\hat{\mathbf{K}}_y$ and $\hat{\mathbf{K}}_r$, the error state vector, $\mathbf{e}(k)$ with closed loop time derivative $\dot{\mathbf{e}}$, is **uniformly ultimately bounded**, and the state $\mathbf{y}$ will converge to a neighborhood of $\mathbf{r}$ (proof in (Ogunmolu et al., 2017, §V.A)).
- Choose

$$\mathbf{V}(\mathbf{e}, \tilde{\mathbf{K}}_y, \tilde{\mathbf{K}}_r^T) = \mathbf{e}^T\mathbf{P}\mathbf{e} + \mathbf{tr}(\tilde{\mathbf{K}}_y^T \boldsymbol{\Gamma}_y^{-1} \tilde{\mathbf{K}}_y^T |\boldsymbol{\Lambda}|) + \mathbf{tr}(\tilde{\mathbf{K}}_r^T \Gamma_r^{-1} \tilde{\mathbf{K}}_r |\boldsymbol{\Lambda}|)$$

- Neural network model $\hat{f}(\mathbf{y}) = \hat{\boldsymbol{\Theta}}^T \boldsymbol{\Phi}(\mathbf{y}) + \varepsilon_f(\mathbf{y})$

Proof Main Matter

$$\dot{\mathbf{V}}(\mathbf{e}, \tilde{\mathbf{K}}_y, \tilde{\mathbf{K}}_r^T) = -\mathbf{e}^T \mathbf{Q} \mathbf{e} - 2\mathbf{e}^T \mathbf{P} \mathbf{B} \boldsymbol{\Lambda} \varepsilon_f$$

$$\dot{\mathbf{V}}(\mathbf{e}, \tilde{\mathbf{K}}_y, \tilde{\mathbf{K}}_r^T) \leq -\lambda_{low} \|\mathbf{e}\|^2 + 2\|\mathbf{e}\| \|\mathbf{P}\mathbf{B}\| \lambda_{high}(\boldsymbol{\Lambda}) \varepsilon_{max}$$

Term Contributions

- $\hat{\mathbf{K}}_y^{\mathbf{T}} \mathbf{y}$ keeps $\mathbf{y} \in \mathbf{B}_R$ stable; $\hat{\mathbf{K}}_r^{\mathbf{T}} \mathbf{r}$ reference tracking
- $\hat{f}(\mathbf{y}, \mathbf{u})$ ensures states starting outside set $\mathbf{y} \in \mathbf{B}_R$ converge to $\mathbf{B}_R$ in finite time

Proof Main Matter

- $\lambda_{low}, \lambda_{high} \equiv$ minimum and maximum characteristic roots of Q and $\boldsymbol{\Lambda}$ respectively
- $\dot{\mathbf{V}}(\cdot)$ is thus negative definite outside the compact set:
  - $\chi = \left(\mathbf{e} : \|\mathbf{e}\| \leq \frac{2\|\mathbf{PB}\|\lambda_{high}(\boldsymbol{\Lambda})\varepsilon_{max}(\mathbf{y})}{\lambda_{low}(\mathbf{Q})} \right)$
- Therefore, the error $\mathbf{e}$ is uniformly ultimately bounded $\mathbf{y}(t) \rightarrow 0$ as $t \rightarrow \infty$

Results

- Choose

$$\mathbf{P} = \begin{bmatrix} -\frac{170500}{2668} & 0 & 0 \\ 0 & -\frac{170500}{2668} & 0 \\ 0 & 0 & -\frac{170500}{2668} \end{bmatrix}$$

- and set

$$\mathbf{B} = \begin{bmatrix} 1 & 1 & 0 & 0 & 0 & 0 \\ 0 & 0 & 1 & 1 & 0 & 0 \\ 0 & 0 & 0 & 0 & 1 & 1 \end{bmatrix}$$

Results

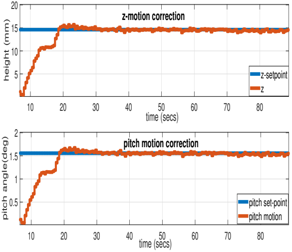

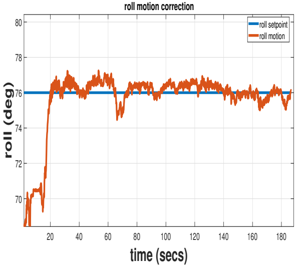

[Left]: Goal command: $(z, \theta, \phi) = (2.5mm, 0.25^\circ, 35^\circ)$ to $(14mm, 1.6^\circ, 45^\circ)^T$. [Right]: Head roll tracking.

Model of a 6-DOF SoRo Mechanism

Page left blank intentionally.

Existing Modeling Approaches

- Finite element modeling: Nesme et al. (2005, 2006); Bern et al. (2017); Gent (2012)
- Constant curvature approaches: Hannan and Walker (2003, 2000); Jones and Walker (2006)
- Piecewise constant curvature model: Jones and Walker (2006)
- Cosserat brothers' beam theory: Renda et al. (2014); Trivedi et al. (2008)
- Non-constant curvature approaches
  - Continuum approximation of hyper-redundant sytems e.g. Mochiyama (2005); Chirikjian and Burdick (1995); Chirikjian (1994),
  - Spring-mass models for semi-rigid robots: Yekutieli et al. (2005); Zheng et al. (2012),
  - Geometric continuum models: Boyer et al. (2006); Gent (2012); Ogden (1997); Sedal et al. (2018); Holzapfel et al. (2000); Rucker et al. (2010); Demirkoparan and Pence (2007)

A Continuum Mechanics Model for IAB Deformation

- **Context**: Model-based approaches generally give better material responses
- **Contributions**
  - Finite elastic (geometric continuum) model for IAB deformation
  - Component stresses, internal pressurization, and particle positions/velocities
  - Synthesis of IAB contact velocities and head motion: manipulation dynamics, selection maps, and contact forces

IAB Kinematics

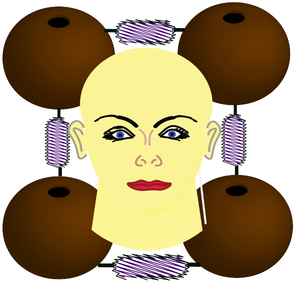

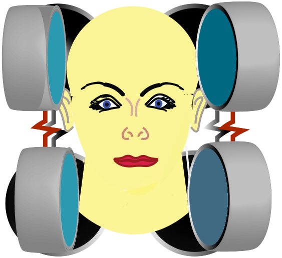

Fibers and deformation

- The rate of deformation from a configuration $\mathcal{B}_0$ to a current configuration $\mathcal{B}$ in component form

$$\mathrm{d}x_i = \frac{\partial x_i}{\partial X_\alpha}\mathrm{d}X_\alpha, \text{ with invariant form } \mathbf{dx} = \mathbf{FdX}$$

$$\text{for an observer } \mathbf{O} \text{ in e.g. basis } \{E_\alpha\}$$

- A *material line element* (a fiber) $\mathbf{dX}$ at a point $\mathbf{X}$ are particles lying along $\mathbf{dX}$ at a point $\mathbf{X}$ of a soft body
- $\mathbf{dX} \neq 0 \implies \mathbf{FdX} \neq 0$ for all $\mathbf{dX} \neq 0$. Therefore, $\mathbf{F}$ must be a non-singular tensor, imposing the restriction, $\det \mathbf{F} \neq 0$

Deformation Analysis of a Soft Continuum Robot

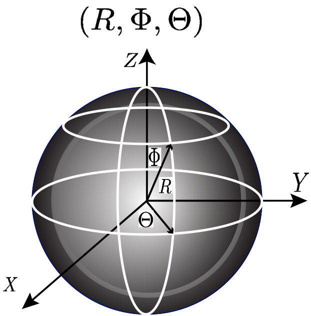

Reference Configuration

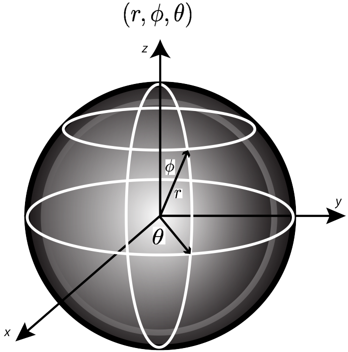

Current Configuration

with

$$R_i \le R \le R_o,\ 0 \le \Theta \le 2\pi,\ 0 \le \Phi \le \pi$$
$$r_i \le r \le r_o,\ 0 \le \theta \le 2\pi,\ 0 \le \phi \le \pi \tag{6}$$

Deformation Analysis

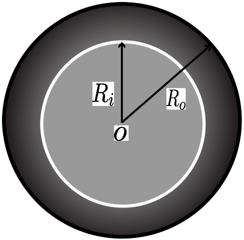

Reference Configuration: (R, Φ, Θ)

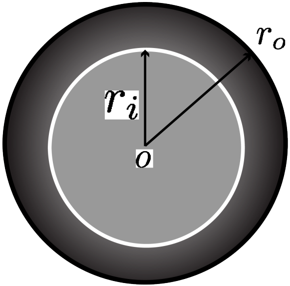

Current Configuration: (r, ϕ, θ)

- An isochoric homogeneous deformation implies

$$\frac{4}{3}\pi\left(R^3 - R_i^3\right) = \frac{4}{3}\pi\left(r^3 - r_i^3\right), \; \theta = \Theta \;\; \phi = \Phi$$

$$r^3 = R^3 + r_i^3 - R_i^3, \;\; \theta = \Theta, \;\; \phi = \Phi \tag{7}$$

Stored Energy Invariants and Principal Ratios

- Spherically symmetric deformation implies coincidence of the *Lagrangean* and *Eulerian* axes
- Thus, principal ratios along azimuthal and zenith axes is $\lambda_\theta = \lambda_\phi = r/R$
- We have $\lambda_r \lambda_\phi \lambda_\theta = 1$ from the incompressibility of the IAB material. Thus, $\lambda_r = \frac{R^2}{r^2}$ so that

$$I_1 = \lambda_r^2 + \lambda_\phi^2 + \lambda_\theta^2, \text{ and } I_2 = \lambda_r^{-2} + \lambda_\phi^{-2} + \lambda_\theta^{-2}. \quad (8)$$

Strain Tensor and Deformation Gradient

- Mooney-Rivlin strain energy form for small deformations:

$$W = \frac{1}{2}C_1(I_1 - 3) + \frac{1}{2}C_2(I_2 - 3). \tag{9}$$

- Deformation gradient in spherical polar coordinates

$$\mathbf{F} = \lambda_r \boldsymbol{e}_r \otimes \boldsymbol{e}_R + \lambda_\phi \boldsymbol{e}_\phi \otimes \boldsymbol{e}_\Phi + \lambda_\theta \boldsymbol{e}_\theta \otimes \boldsymbol{e}_\Theta$$

$$\mathbf{F} = \frac{R^2}{r^2}\boldsymbol{e}_r \otimes \boldsymbol{e}_R + \frac{r}{R}\boldsymbol{e}_\phi \otimes \boldsymbol{e}_\Phi + \frac{r}{R}\boldsymbol{e}_\theta \otimes \boldsymbol{e}_\Theta. \tag{10}$$

$\mathbf{B} = \mathbf{F}\,\mathbf{F}^T$:= Left Cauchy-Green deformation tensor

$\mathbf{C} = \mathbf{F}^T\mathbf{F}$:= Right Cauchy-Green deformation tensor

Stress Laws and Constitutive Equations

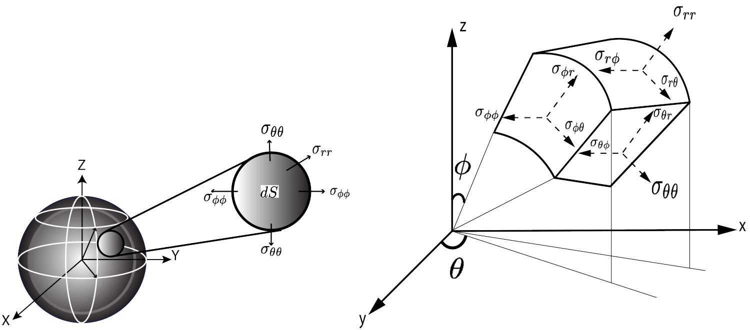

Stress distribution on the internal continuum's differential surface, *dS*.

Invariants of Deformation

$$I_1 = \mathbf{tr}(\mathbf{C}) = \frac{R^4}{r^4} + \frac{2\,r^2}{R^2};\; I_2 = \mathbf{tr}\left(\mathbf{C}^{-1}\right) = \frac{r^4}{R^4} + \frac{2\,R^2}{r^2}. \tag{11}$$

For a constrained elastic material, we have the following constitutive relation

$$\begin{aligned}\boldsymbol{\sigma} &= \mathbf{G}(\mathbf{F}) + q\mathbf{F}\frac{\partial \boldsymbol{\Lambda}}{\partial \mathbf{F}}(\mathbf{F}) \\ &= \mathbf{G}(\mathbf{F}) - p\mathbf{F}\mathbf{F}^{-T}\det(\mathbf{F}) \\ &= \mathbf{G}(\mathbf{F}) - p\mathbf{I} \end{aligned} \tag{12}$$

Cauchy stress and hydrostatic pressure

In terms of the stored strain energy, we have the stress tensor field as

$$\boldsymbol{\sigma} = \begin{bmatrix} \sigma_{rr} & \sigma_{r\phi} & \sigma_{r\theta} \\ \sigma_{\phi r} & \sigma_{\phi\phi} & \sigma_{\phi\theta} \\ \sigma_{\theta r} & \sigma_{\theta\phi} & \sigma_{\theta\theta} \end{bmatrix} = \frac{\partial W}{\partial \mathbf{F}} \mathbf{F}^T - p\mathbf{I}, \tag{13}$$

or

$$\boldsymbol{\sigma} = C_1 \mathbf{B} - C_2 \mathbf{C}^{-2} - p\mathbf{I} \tag{14}$$

where C_1, C_2 are appropriate choices of the IAB material moduli;

$$\sigma_{rr} = -p + C_1 \frac{R^4}{r^4} - C_2 \frac{r^8}{R^8} \tag{15a}$$

$$\sigma_{\theta\theta} = \sigma_{\phi\phi} = -p + C_1 \frac{r^2}{R^2} - C_2 \frac{R^8}{r^8} \tag{15b}$$

Contact-Free BVP for IAB Deformation

- Consider an IAB with boundary conditions,

$$\sigma_{rr}\big|_{R=R_o} = -P_{\text{atm}}, \quad \sigma_{rr}\big|_{R=R_i} = -P_{\text{atm}} - P \tag{16}$$

- If the stress components, σ_{ij}, satisfy hydrostatic equilibrium, equilibrium equations for the body force $\boldsymbol{b}'s$ physical component vectors, b_r, b_θ, b_ϕ are

$$-b_r = \frac{1}{r^2}\frac{\partial}{\partial r}(r^2\sigma_{rr}) + \frac{1}{r\sin\phi}\frac{\partial}{\partial\phi}(\sin\phi\sigma_{r\phi}) + \frac{1}{r\sin\phi}\frac{\partial}{\partial\theta}(\sigma_{r\theta}) - \frac{1}{r}(\sigma_{\theta\theta} + \sigma_{\phi\phi}) \tag{17a}$$

$$-b_\phi = \frac{1}{r^3}\frac{\partial}{\partial r}(r^3\sigma_{r\phi}) + \frac{1}{r\sin\phi}\frac{\partial}{\partial\phi}(\sin\phi\sigma_{\phi\phi}) + \frac{1}{r\sin\phi}\frac{\partial}{\partial\theta}(\sigma_{\theta\phi}) - \frac{\cot\phi}{r}(\sigma_{\theta\theta}) \tag{17b}$$

$$-b_\theta = \frac{1}{r^3}\frac{\partial}{\partial r}(r^3\sigma_{\theta r}) + \frac{1}{r\sin^2\phi}\frac{\partial}{\partial\phi}(\sin^2\phi\sigma_{\theta\phi}) + \frac{1}{r\sin\phi}\frac{\partial}{\partial\theta}(\sigma_{\theta\theta}) \tag{17c}$$

- Cauchy's 1st law of motion

$$\text{div}\,\boldsymbol{\sigma}^T + \rho\mathbf{b} = \rho\dot{\mathbf{v}} \tag{18}$$

Stress at Hydrostatic Equilibrium

- Equilibrium therefore implies that

$$\mathbf{div}\ \boldsymbol{\sigma} = 0$$

$$\frac{1}{r}\frac{\partial}{\partial r}(r^2\sigma_{rr}) = (\sigma_{\theta\theta} + \sigma_{\phi\phi})$$

- Whereupon,

$$P = 2C_1 \int_{R_i}^{R_\circ} \left(\frac{1}{r} - \frac{R^6}{r^7}\right) dR + 2C_2 \int_{R_i}^{R_\circ} \left(\frac{r^5}{R^6} - \frac{R^{10}}{r^{11}}\right) dR$$
$$\equiv \int_{r_i}^{r_\circ} \left[2C_1 \left(\frac{r}{R^2} - \frac{R^4}{r^5}\right) + 2C_2 \left(\frac{r^7}{R^8} - \frac{R^8}{r^9}\right)\right] dr. \tag{19}$$

- (19) completely determines the deformation kinematics of the IAB material at rest.

Example I: IAB Deformation (Extension)

Deformation Parameters		
$C_1 = 11,000$	$C_2 = 22,000$	$R_i = 10cm,\ r_i = 13cm$
$R_\circ = 15cm$	$r_\circ = 16.60cm$	$P = 14.52psi$

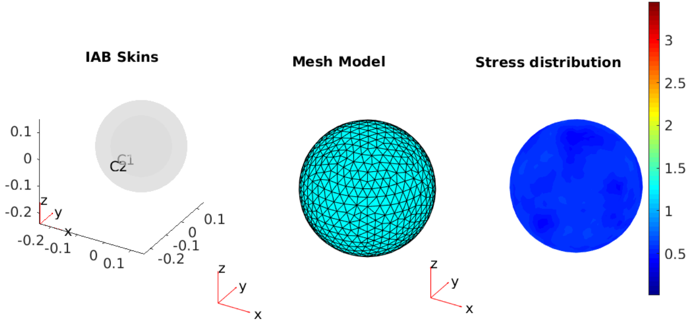

Example I: Deformation (Extension) Results

Mesh Time: 0.8838s	Total Time: 4.7782s
$\nu = 0.45$	$\rho = 9.8446 \times 10^{-4} kG/m^3$

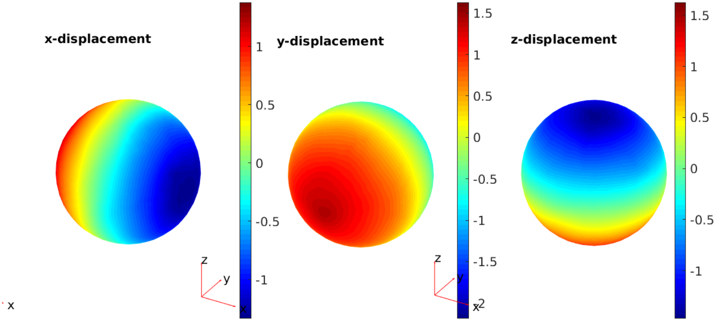

Example II: IAB Deformation (Extension)

Deformation Parameters		
$C_1 = 500,000$	$C_2 = 1,000,000$	$R_i = 7.5cm,\ r_i = 12cm$
$R_{\circ} = 10cm$	$r_{\circ} = 13.21cm$	$P = 14.5193psi$

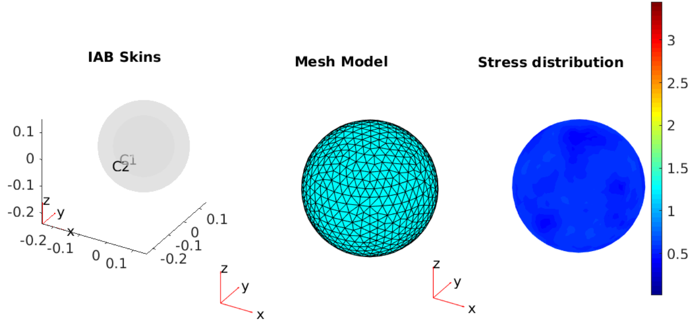

Example II: Deformation Results (Extension)

Mesh Time: .9143s	Total Time: 4.1445s
$\nu = 0.4995$	$\rho = 10^{-4}\ kg/m^3$

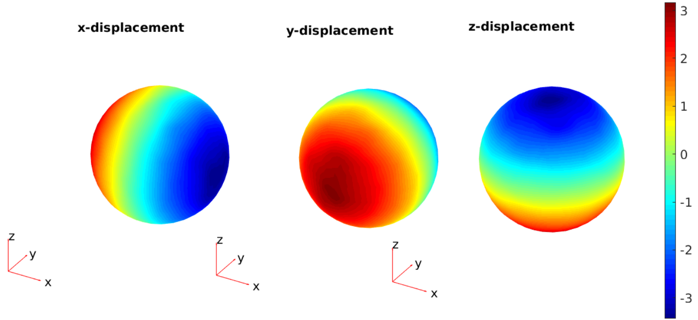

Example III: IAB Deformation (Compression)

Deformation Parameters		
$C_1 = 500,000$	$C_2 = 1,200,000$	$R_i = 12cm,\ r_i = 10cm$
$R_\circ = 15cm$	$r_\circ = 13.83cm$	$P = -27.3631$ psi

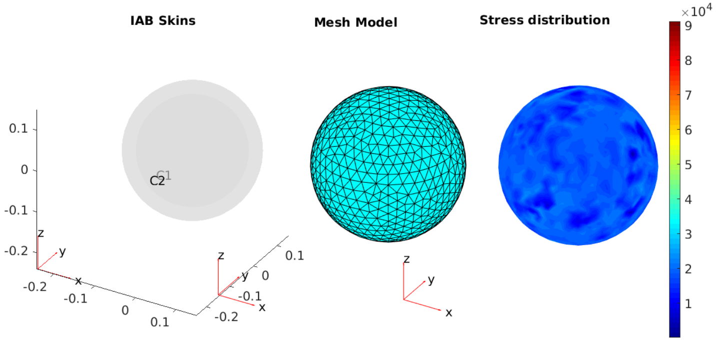

Example III: Deformation Results (Compression)

Mesh Time: .8625s	Total Time: 4.5338s
$\nu = 0.45$	$\rho = 12 \times 10^{-4}\ kg/m^3$

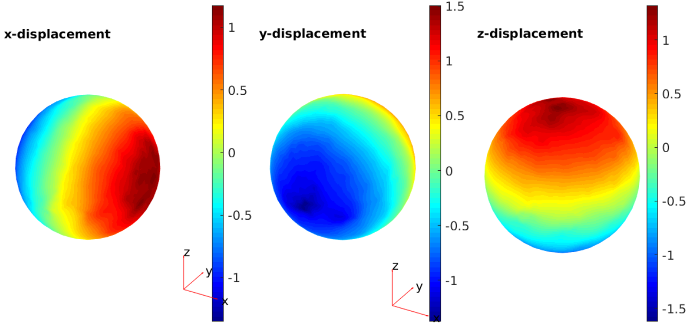

Example IV: IAB Deformation (Compression)

Deformation Parameters		
$C_1 = 1.1e12$	$C_2 = 2.2e10$	$R_i = 10cm,\ r_i = 8cm$
$R_\circ = 19cm$	$r_\circ = 18.54cm$	$P = -27.3631\text{psi}$

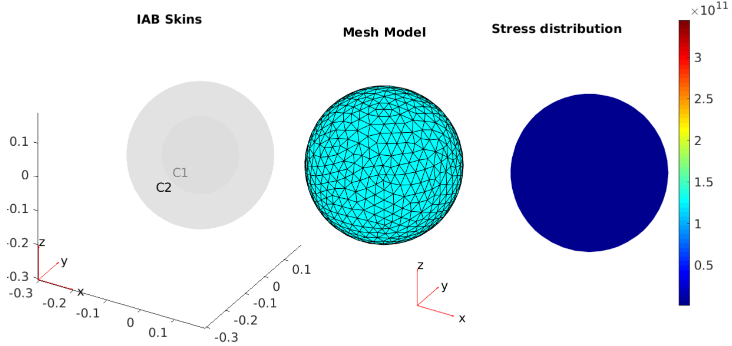

Example IV: Deformation Results (Compression)

Mesh Time: 0.823576s	Total Time: 4.5098s
$\nu = 0.495$	$\rho = 2.0 \times 10^{-5}\ kg/m^3$

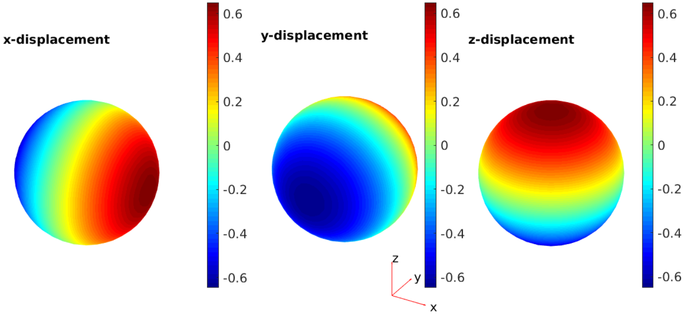

Multi-DOF IAB Kinematics & Dynamics

- **Outline**
  - Solve boundary-value problem for IAB kinematics with head contact
  - Relate Deformation Kinematics to Contact Dynamics
  - Derive head velocity and orientation in terms of contact velocities
  - Derive Newton-Euler's Dynamics of the Head-IAB system for control

Contact Kinematics

- All friction cones lie within a soft contact type model: Nguyen (1988)

$$FC = \{f_c \in \mathbb{R}^n : \|f^t_{c_{ij}}\| \le \mu_{ij} \|f^n_{c_i}\|, \quad i = 1, \ldots, k, \quad j = 1, \ldots, m_i\} \tag{20}$$

- $f^t_{c_{ij}}$ = tangent component of j^{th} element of contact force
- $f^n_{c_i}$ = i^{th} contact's normal force, and μ_{ij} is $f_{c_{ij}}$'s coefficient of friction
- Contact force within friction cone:

$$\tilde{F}_{c_i} = \begin{bmatrix} \mathbf{I} & 0 \\ 0 & n_{c_i} \end{bmatrix} \begin{bmatrix} f_{c_i} \\ \tau_{c_i} \end{bmatrix}, \tag{21}$$

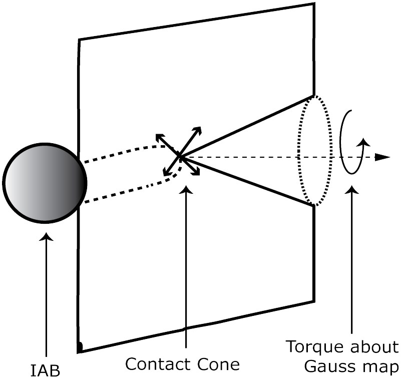

IAB-Head Soft Contact

Contact Map

- Soft contact type is the map

$$G_i(r_{c_i}, \xi_h) = \begin{bmatrix} \mathbf{I} & \mathbf{0} \\ \hat{\omega}(r_{c_i}) & \mathbf{I} \end{bmatrix} B_i(\xi_h, \xi_r) \tag{22}$$

- Head never rolls out of convex sum of conic forces of individual IABs
- For multiple IABs acting on the head, resultant head force is a superposition of individual IAB forces

$$\tilde{F}_h = \left[G_1, \ldots, G_8\right] \begin{pmatrix} \tilde{F}_{c_1} \\ \tilde{F}_{c_8} \end{pmatrix} = G\tilde{F}_c, \tag{23}$$

- where $F_h \in \mathbb{R}^6$ and $F_c \in \mathbb{R}^{m_1} \times \mathbb{R}^{m_2} \times \ldots \times \mathbb{R}^{m_8}$

BVP for IAB-Head Dynamics

- Velocity constraint dual

$$\begin{pmatrix} \tilde{v}_{c_i} \\ \tilde{\omega}_{c_i} \end{pmatrix} = \begin{bmatrix} \mathbf{I} & \hat{\omega}(r_{c_i}) \\ 0 & \mathbf{I} \end{bmatrix} \begin{pmatrix} v_{c_h} \\ \omega_{c_h} \end{pmatrix}. \tag{24}$$

- If v_c is the conjugate velocity to f_c, then forces exerted by the fingers are

$$\begin{pmatrix} v_c \\ \omega_c \end{pmatrix} = G^T \begin{pmatrix} v_h \\ \omega_h \end{pmatrix} \tag{25}$$

- Equations of motion for IAB continuum

$$\dot{\rho} + \rho \mathrm{div}\mathbf{v} = 0, \tag{26a}$$

$$\boldsymbol{\sigma}^T = \boldsymbol{\sigma}, \tag{26b}$$

$$\mathrm{div}\boldsymbol{\sigma}^T + \rho\boldsymbol{b} = \rho\dot{\mathbf{v}} \tag{26c}$$

IAB Forces under Entropy

Head forces (see derivation in (Ogunmolu, 2019, Appendix C.)) are in part the internal pressurization, P_i, and the stress tensor components $\{\sigma_{\phi\phi}(\epsilon), \sigma_{\theta\theta}(\zeta)\}$,

$$\begin{aligned} P = \int_{r_i}^{r_o} \Bigg[\frac{1}{r} \left(-2p + 2C_1 \frac{r^2}{R^2} - 2C_2 \frac{R^8}{r^8} \right) - \rho b_r + \rho \cos\theta \left(2\dot{r}\dot{\phi}\cos\theta + r\cos\theta\ddot{\phi} - 2r\dot{\theta}\dot{\phi}\sin\theta \right) \\ -\rho \sin\phi \left(\cos\theta(-\ddot{r} + r\dot{\theta}^2 + r\dot{\phi}^2) + \sin\theta(2\dot{r}\dot{\theta} + r\ddot{\theta}) \right) \Bigg] dr \end{aligned} \tag{27a}$$

$$\begin{aligned} \sigma_{\phi\phi}(\epsilon) = -\int_{\epsilon}^{\pi} \Big[r\rho \Big[\cos\phi \left(2r\dot{\theta}\dot{\phi}\cos\theta + (2\dot{r}\dot{\phi} + r\ddot{\phi})\sin\theta \right) + \\ \sin\theta \left(2\dot{r}\dot{\theta}\cos\theta + r\ddot{\theta}\cos\theta + (\ddot{r} - r\dot{\theta}^2 - r\dot{\phi}^2) \right) \sin\phi \Big] - \rho r b_\theta \Big] d\phi, \; 0 \le \epsilon \le \pi \end{aligned} \tag{27b}$$

$$\sigma_{\theta\theta}(\zeta) = -\int_{\zeta}^{2\pi} \left[-r\rho b_\theta \sin\phi + r\rho\sin\phi\cos\phi \left(\ddot{r} - r\dot{\phi}^2 \right) - r\rho\sin^2\phi \left(2\dot{r}\dot{\phi} + r\ddot{\phi} \right) \right] d\theta, \; 0 \le \zeta \le 2\pi \tag{27c}$$

where $0 \le \epsilon \le \pi, 0 \le \zeta \le 2\pi$ and gravity forces.

Piola-Kirchoff Stress Tensor & Contact Forces

- For an infinitesimal vector element $\mathbf{dA}$ in $\mathcal{B}_0$, we have $\mathbf{dA} = \mathbf{N}\mathrm{dA}$ for a surface dA with outward normal map $\mathbf{N}$
- Similarly, in configuration $\mathcal{B}$, $\mathbf{da} = \mathbf{n}\,\mathrm{da}$ for an outward normal map $\mathbf{n}$
- Therefore on the IAB boundary, volume preservation implies that

$$\int_{\partial\mathcal{B}} \boldsymbol{\sigma}\,\mathbf{n}\,\mathrm{da} = \int_{\partial\mathcal{B}_\circ} J\,\boldsymbol{\sigma}\,\mathbf{H}\,\mathbf{N}\,\mathrm{dA}. \tag{28}$$

- Define the Piola-Kirchoff stress tensor field

$$\mathbf{S} = J\,\mathbf{H}^T\,\boldsymbol{\sigma} \quad \text{where} \quad \mathbf{H} = \mathbf{F}^{-T} \tag{29}$$

- It follows that

$$\boldsymbol{\sigma}\mathbf{da} = \mathbf{S}^T\mathbf{dA}.$$

Contact force and stress fields

Contact Wrench

$$f_{c_i} = \mathbf{S}_i^T \mathbf{dA}_i = J_i \boldsymbol{\sigma}_i \mathbf{H}_i \mathbf{dA}_i = J_i \boldsymbol{\sigma}_i \mathbf{F}_i^{-1} \mathbf{dA}_i \tag{30}$$

$$\boldsymbol{\tau}_{c_i} = f_{c_i} \times r_{c_i} \tag{31}$$

whereupon,

$$f_{c_i} = \left(\frac{R_i^2}{r_i^2} P_i + \frac{R_i}{r_i} \sigma_{\phi\phi_i}(\epsilon) + \frac{R_i}{r_i} \sigma_{\theta\theta_i}(\zeta) \right) n_{c_i} dA_i \tag{32}$$

and the contact force map is

$$\tilde{F}_{c_i} = \begin{bmatrix} \mathbf{I} & 0 \\ 0 & n_{c_i} \end{bmatrix} \begin{bmatrix} f_{c_i} \\ f_{c_i} \times r_{c_i} \end{bmatrix}. \tag{33}$$

Contact coordinates and head motion

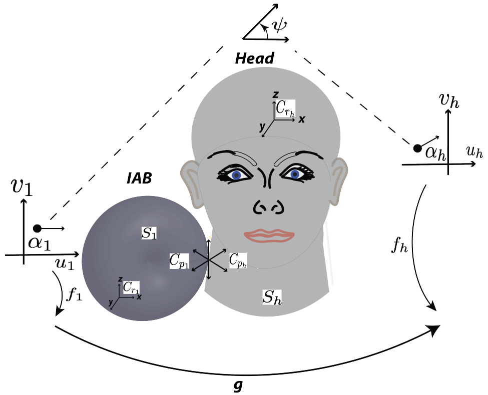

$$\alpha_1 = (u_1, v_1) \in U_1, \text{ and } \alpha_h = (u_h, v_h) \in U_h$$

$$f_i(u_i, v_i) : \{U \to S_i \subset \mathbb{R}^3 | i = 1, h\}.$$

Differential Geometry of Contact Coordinates

- Define contact coordinates $\eta = (\alpha_1, \alpha_h, \psi)$
- Let $g \in \Omega \subset SE(3)$ and let $R \in SO(3)$ be g's rotatory component
- $\Omega = \{\{S_{1_i}\}_{i=1}^{n_1}, \{S_{h_i}\}_{i=1}^{n_h}\}$ for which the IAB and head remain in contact
- At a point of contact, η must satisfy

$$g \circ f_1(\alpha_1) = f_h(\alpha_h) \tag{34a}$$
$$R\, n_1(\alpha_1) = -n_h(\alpha_h) \tag{34b}$$

- Additionally, the orientation of the tangent planes of α_1 and α_h imply that

$$R \frac{\partial f_1}{\partial \alpha_1} M_1^{-1} R_\psi = \frac{\partial f_h}{\partial \alpha_h} M_h^{-1} \tag{35}$$

- Hence, we have the contact equations (see derivation in Ogunmolu (2019))

$$\dot{\alpha}_h = M_h^{-1}(\mathcal{K}_h + \tilde{\mathcal{K}}_1)^{-1} \left(\omega_t - \tilde{\mathcal{K}}_1 v_t\right) \tag{36a}$$
$$\dot{\alpha}_1 = M_1^{-1} R_\psi (\mathcal{K}_h + \tilde{\mathcal{K}}_1)^{-1} (\omega_t - \mathcal{K}_h v_t) \tag{36b}$$
$$\dot{\psi} = \omega_n + T_h M_h \dot{\alpha}_h + T_1 M_1 \dot{\alpha}_1 \tag{36c}$$

Contact Equations

where

$$M_i = \begin{bmatrix} \| \frac{\partial f_i}{\partial u_i} \| & 0 \\ 0 & \| \frac{\partial f_h}{\partial v_i} \| \end{bmatrix}, \qquad R_\psi = \begin{bmatrix} \cos\psi & -\sin\psi \\ -\sin\psi & -\cos\psi \end{bmatrix} \tag{37a}$$

$$T_h = y_h^T \frac{\partial x_h}{\partial \alpha_h} M_h^{-1}, \qquad T_1 = y_1^T \frac{\partial x_1}{\partial \alpha_1} M_1^{-1}, \; \omega_n = z_h^T \omega \tag{37b}$$

$$\mathcal{K}_h = \left[x_h^T, \quad y_h^T \right]^T \frac{\partial n_h^T}{\partial \alpha_h} M_h^{-1}, \qquad \mathcal{K}_1 = R_\psi \left[x_1^T, \quad y_1^T \right]^T \frac{\partial n_1^T}{\partial \alpha_1} M_1^{-1} R_\psi \tag{37c}$$

$$\omega_t = \left[x_h^T, \quad y_h^T \right]^T \left[n_h \times \omega \right]^T, \qquad v_t = \left[x_h^T, \quad y_h^T \right]^T \left[(-f_h \times \omega + v) \right]^T. \tag{37d}$$

Multi-IAB Kinematics

- IAB configuration space with respect to the spatial frame at a certain time can then be described by $g_{st}(\mathbf{r}) : \mathbf{r} \rightarrow g_{st}(\mathbf{r}) \in SE(3)$
- Strain state of the IAB is characterized by the strain field

$$\hat{\xi}_i(\mathbf{r}) = g_i^{-1} \frac{\partial g_i}{\partial \mathbf{r}} \in \mathfrak{se}(3) = g_i^{-1} g_i' \tag{38}$$

- g_i': tangent vector at g_i such that $g_i' \in T_{g_i(\mathbf{r})} SE(3)$
- IAB's strain field as an exponential map of $SE(3)$

$$g_i(\mathbf{r}) = \exp^{\|\mathbf{r}\| \hat{\xi}_i} = \mathbf{I} + \hat{\xi}_i \|\mathbf{r}\| + \frac{\hat{\omega}}{\|\omega\|^2} \left(1 - \cos(\|\mathbf{r}\| \|\omega\|)\right) \hat{\xi}_i^2 + \frac{\hat{\omega}^3}{\|\omega\|^3} \left(\|\mathbf{r}\| \|\omega\| - \sin(\|\mathbf{r}\| \|\omega\|)\right) \hat{\xi}_i^3. \tag{39}$$

Forward Kinematics

- FK Jacobian:

$$\begin{pmatrix} v_{iab_i} \\ \omega_{iab_i} \end{pmatrix} = \frac{\partial K_{iab_i}}{\partial \mathbf{r}_i} \frac{d\mathbf{r}}{dt} K_{iab_i}^{-1} = \boldsymbol{J}_i(\mathbf{r}_i)\dot{\mathbf{r}}_i \tag{40}$$

- Contact forces/velocities mapped by the contact Jacobian:

$$\boldsymbol{J}_{c_i}(\xi_h, \xi_{iab_i}) = \begin{bmatrix} \mathbf{I} & \hat{\boldsymbol{\omega}}(r_{c_i}) \\ \mathbf{0} & \mathbf{I} \end{bmatrix} J_{r_i}, \tag{41}$$

- where $\boldsymbol{J}_{c_i} : \dot{\xi}_{r_i} \to \begin{bmatrix} v_{c_i}^T, & \omega_{c_i}^T \end{bmatrix}^T$
- $\xi_r = (\xi_{r_1}, \xi_{r_2}, \cdots, \xi_{r_8})$: positions and orientations for each of the 8 IABs

Manipulation Map

- For a *selection matrix* $B_i^T(\xi_h, \xi_{iab_i}) \in \mathbb{R}_i^m$ for a particular manipulation task

$$G_i^T(\xi_h, \xi_{iab_i})\xi_h = B_i^T(\xi_h, \xi_{iab_i})\boldsymbol{J}_{c_i}(\xi_h, \xi_{r_i})\dot{\xi}_{iab_i} \tag{42}$$

- Manipulation constraint:

$$\begin{bmatrix} G_1^T \\ G_2^T \\ \vdots \\ G_8^T \end{bmatrix} \begin{pmatrix} v_h \\ \omega_h \end{pmatrix} = \begin{bmatrix} B_1^T\boldsymbol{J}_{c_1} & 0 & \cdots & 0 \\ 0 & B_2^T\boldsymbol{J}_{c_2} & \cdots & 0 \\ \vdots & \vdots & \ddots & \vdots \\ 0 & 0 & \cdots & B_8^T\boldsymbol{J}_{c_8} \end{bmatrix} \begin{pmatrix} \dot{\mathbf{r}}_{iab_1} \\ \dot{\mathbf{r}}_{iab_2} \\ \vdots \\ \dot{\mathbf{r}}_{iab_8} \end{pmatrix} \tag{43}$$

Planar Manipulation Example

$$G_2 = \begin{bmatrix} \mathbf{I} & 0 \\ \hat{\omega}\begin{pmatrix} -r_{c_2}\sin\phi_2 \\ r_{c_2}\cos\phi_2 \\ 0 \end{pmatrix} & \mathbf{I} \end{bmatrix} \begin{pmatrix} 1 & 0 \\ 0 & 1 \\ 0 & 0 \\ 0 & 0 \\ 0 & 0 \\ 0 & 0 \end{pmatrix}$$

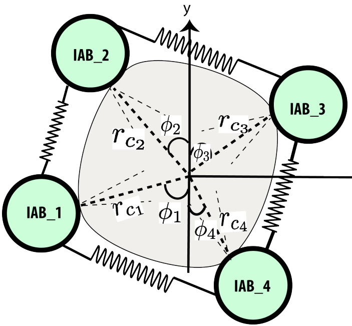

$$G_1 = \begin{bmatrix} \mathbf{I} & 0 \\ \hat{\omega}\begin{pmatrix} -r_{c_1}\sin\phi_1 \\ -r_{c_1}\cos\phi_1 \\ 0 \end{pmatrix} & \mathbf{I} \end{bmatrix} \begin{pmatrix} 1 & 0 \\ 0 & 1 \\ 0 & 0 \\ 0 & 0 \\ 0 & 0 \\ 0 & 0 \end{pmatrix}$$

Head Planar Manipulation Map

$$G_3 = \begin{bmatrix} & \mathbf{I} & 0 \\ \hat{\omega} & \begin{pmatrix} r_{c_3}\sin\phi_3 \\ r_{c_3}\cos\phi_3 \\ 0 \end{pmatrix} & \mathbf{I} \end{bmatrix} \begin{pmatrix} 1 & 0 \\ 0 & 1 \\ 0 & 0 \\ 0 & 0 \\ 0 & 0 \\ 0 & 0 \end{pmatrix} \qquad G(x, y, \phi) = \begin{bmatrix} 1 & 0 & r_{c_1}\cos\phi_1 \\ 0 & 1 & -r_{c_1}\sin\phi_1 \\ 1 & 0 & -r_{c_2}\cos\phi_2 \\ 0 & 1 & -r_{c_2}\sin\phi_2 \\ 1 & 0 & -r_{c_3}\cos\phi_3 \\ 0 & 1 & r_{c_3}\sin\phi_3 \\ 1 & 0 & r_{c_4}\cos\phi_4 \\ 0 & 1 & r_{c_4}\sin\phi_4 \end{bmatrix}^T$$

where $G(\cdot)$ is the manipulation map for all forces with respect to xy coordinates.

Multi-IAB Lagrangian Dynamics

$$L(\mathbf{r}, \dot{\mathbf{r}}) = T(\mathbf{r}, \dot{\mathbf{r}}) - V(\mathbf{r}). \tag{44}$$

- Pneumatic system equation

$$\frac{d}{dt}\frac{\partial L}{\partial \dot{\mathbf{r}}_i} - \frac{\partial L}{\partial \mathbf{r}_i} = \boldsymbol{\tau}_i, \quad i = 1, \ldots, m \tag{45}$$

- Define the Eulerian strain rate tensor

$$\boldsymbol{\Gamma} = \text{grad } \mathbf{v}(\mathbf{r}, t). \tag{46}$$

- Dropping explicit time-dependence, we have from Cauchy's first law

$$\text{div } (\boldsymbol{\sigma}^T \mathbf{v}) - \mathbf{tr}(\boldsymbol{\sigma}\,\boldsymbol{\Gamma}) + \rho\mathbf{b} \cdot \mathbf{v} = \rho\mathbf{v} \cdot \dot{\mathbf{v}}. \tag{47}$$

Balance of mechanical energy

$$\int_{\mathcal{B}} \rho \mathbf{b} \cdot \mathbf{v}\, dv + \int_{\partial \mathcal{B}} f_\rho \cdot \mathbf{v}\, da = \frac{d}{dt} \int_{\mathcal{B}} \frac{1}{2} \rho \mathbf{v} \cdot \mathbf{v}\, dv + \int_{\mathcal{B}} \mathbf{tr}(\boldsymbol{\sigma}\, \boldsymbol{\Gamma})\, dv \tag{48}$$

- Taking cognizance that $\boldsymbol{\Sigma} = \frac{1}{2}(\boldsymbol{\Gamma} + \boldsymbol{\Gamma}^T)$, we have

$$T(\mathbf{r}, \dot{\mathbf{r}}) = \frac{1}{2} \rho \mathbf{v} \cdot \mathbf{v}, \quad V(\mathbf{r}) = \mathbf{tr}(\boldsymbol{\sigma}\, \boldsymbol{\Sigma}). \tag{49}$$

- whereupon, we find that

$$\boldsymbol{\tau} = \begin{bmatrix} \rho & 0 & 0 \\ 0 & \rho\, r^2 & 0 \\ 0 & 0 & \rho\, r^2 \sin^2 \phi \end{bmatrix} \begin{bmatrix} \ddot{r} \\ \ddot{\phi} \\ \ddot{\theta} \end{bmatrix} + \mathbf{diag} \begin{bmatrix} 2\, \rho\, r \left(\dot{\theta}\, \sin^2 \phi + \dot{\phi} \right) \\ \rho r \left(r \dot{\theta} \sin 2\phi - \dot{\phi} \right) \\ -\rho r \dot{\theta} \sin \phi \,(r \cos \phi + \sin \phi) \end{bmatrix} \begin{bmatrix} \dot{r} \\ \dot{\phi} \\ \dot{\theta} \end{bmatrix} \tag{50}$$

- Compactly, we write the IAB actuator dynamics as

$$M_{iab_j}(r_j, \phi_j) \ddot{\mathbf{r}}_j + C_{iab_j}(r_j, \phi_j, \dot{\theta}_j, \dot{\phi}_j) \dot{\mathbf{r}}_j = \boldsymbol{\tau}_j \tag{51}$$

Newton-Euler Equations for IAB-Head System

- No actuator torques:

$$\boldsymbol{M}_h(\zeta)\ddot{\zeta} + \boldsymbol{C}_h(\zeta, \dot{\zeta})\dot{\zeta} + \boldsymbol{N}_h(\zeta, \dot{\zeta}) = 0 \tag{52}$$

- Manipulation constraint:

$$G^T(\zeta, \mathbf{r})\dot{\zeta} = \boldsymbol{J}(\zeta, \mathbf{r})\dot{\mathbf{r}}. \tag{53}$$

- Wherefore, we find that

$$\left(\frac{d}{dt}\frac{\partial L}{\partial \dot{\zeta}} - \frac{\partial L}{\partial \zeta}\right)\delta\zeta + GJ^{-T}\left(\frac{d}{dt}\frac{\partial L}{\partial \dot{\mathbf{r}}} - \frac{\partial L}{\partial \mathbf{r}}\right) = GJ^{-T}\boldsymbol{\tau} \tag{54}$$

- Equations (54) and (53) completely describe the system.

This page is left blank intentionally.

BOO, FMO

- Aim high-precision, geometrically-shaped photons to tumors

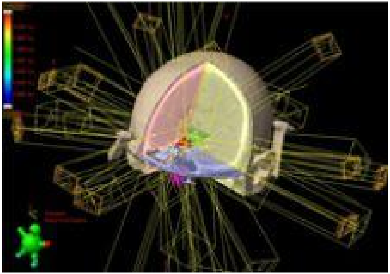

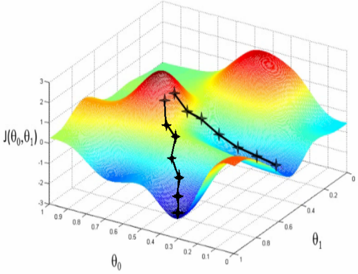

Reprinted from David Shepard's AAPM Slides

- Beamlets from photons; optimal beam angles; FMO process ▷ intensity modulation

Existing Approaches

- Stochastic optimization approaches (SA, GA): Bortfeld and Schlegel (1993); Södertröm and Brahme (1993); Pugachev et al. (2000); Pugachev and Xing (2002); Aleman et al. (2008); Bertsimas et al. (2013)
- Gradient search: Stein et al. (1997); Craft (2007); Bertsimas et al. (2013)
- Feature-based machine learning: Lu et al. (2006); Li and Lei (2010)
- Mixed-integer LP, branch and cut, beam angle elimination algorithms: Wang et al. (2003); D D'Souza et al. (2004); Lim et al. (2007); Jia et al. (2011)

An ADP + Monte-Carlo Evaluation Proposal

- **Context**: For 180 discretized angles in a 5 beam plan, there are $188,956,800,000$ possible search directions
- **Proposal**
  - Monte-Carlo game planning strategy
  - Deep neural network policy: map patients geometry to beam angles
  - Refine accuracy of beams selection policy with fictitious self-play [Heinrich et al. (2015)]

State Representation: Network Input Plane

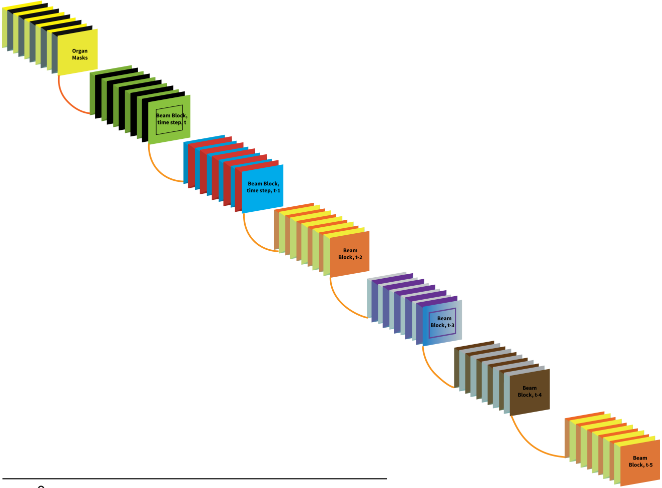

[0] Net policy: produces a subjective probability distribution about a rational decision-making agent's preference for a *lottery* (or *value*) in an uncertain environment. With new information, decision-maker's subjective probability distribution gets revised. Repeatedly sampling from this probability distribution enables the transition between episode contexts, *i.e.*, $\mathbf{x}_k \to \mathbf{x}_{k+1}$

Two-Player Framework

- Players base their decisions on a random event's outcome
- Guided by a nonstationary Markovian policy set $\Pi^{p_i} = \{\Pi^{p_1}, \Pi^{p_2}\}$ such that
  - $\boldsymbol{\pi}^{p_1} \in \{\pi_0^{p_1}, \pi_1^{p_1}, \ldots, \pi_T^{p_1}\} \subseteq \Pi^{p_1}$
  - $\boldsymbol{\pi}^{p_2} \in \{\pi_0^{p_2}, \pi_1^{p_2}, \ldots, \pi_T^{p_2}\} \subseteq \Pi^{p_2}$
- **Stochastic action selection strategy** $\boldsymbol{\pi}(u|\mathbf{x}) := \{\boldsymbol{\pi}^{p_1}, \boldsymbol{\pi}^{p_2}\}$ contain control sequences $\{u_t^{p_1}\}_{0\leq t\leq T}$ and $\{u_t^{p_2}\}_{0\leq t\leq T}$

Cost-to-go

- Optimal **cost-to-go** value function for state

$$V_t^*(\mathbf{x}) = \inf_{\pi^{p_1} \in \prod^{p_1}} \sup_{\pi^{p_2} \in \prod^{p_2}} \mathbb{E}\left[\sum_{t=i}^{T-1} V_t(\mathbf{x}_0, f(\mathbf{x}_t, \pi^{p_1}, \pi^{p_2}))\right],$$
$$\mathbf{x} \in \mathbf{X};\ V_T^*(\mathbf{x}) = 0,\ \forall\, \mathbf{x} \in \mathbf{X}$$

- Each player generates a **mixed strategy** determined by **averaging the outcome** of individual plays
- Find optimal saddle point control pair $\{u_t^{p_1^*}, u_t^{p_2^*}\}$ such that

$$V_{p_1}^\star \le V_t^\star \le V_{p_2}^\star \quad \forall\, \{\pi_t^{p_1}, \pi_t^{p_2}\}_{0 \le t \le T}.$$

Game Tree Simulation

- Network roll-out policy guides a tree's game, Γ, toward a *best-first* set of beam angle candidates
- Essentially, a sampling-based lookout algorithm
  - Focus on state space regions with least FMO score for beam angle combinations
  - Lookout simulation steps: **Selection**; **Expansion**; **Simulation**; **Back-up**
  - A 'best move' for current beam block selected, after each iteration

[0] *Selection*: from root node, recursively apply child selection policy to navigate tree branches until an expandable node is encountered. *Expansion*: iteratively add one or more children to the current node, based on the available move probabilities.

Fluence Map Optimization (FMO)

- Suppose $\mathcal{X}$ is the total discretized *VOI*'s in a target volume
- Suppose $\mathcal{B}_1 \cup \mathcal{B}_2 \cup \ldots \cup \mathcal{B}_n \subseteq \mathcal{B}$ represents the partition subset of a beam $\mathcal{B}$
- Suppose further that $\mathcal{D}_{ij}(\theta_k)$ is the matrix that describes each dose influence, d_i.
- $\mathcal{D}_{ij}(\theta_k)$ is computed for each dose to voxel i occupying a bixel, j, incident from a beam angle, θ_k at every $360°/\varphi°$. NB: $j \in \theta_k$

The FMO Problem

- Pre-calculated dose term:
  $\mathbf{Ax} = \{\sum_s \frac{w_s}{v_s}\mathcal{D}_{ij}^s \mathbf{x}_s \,|\, \mathcal{D}_{ij}^s \in \mathbb{R}^{n \times l}, n \gg l\}$

- Find decision variable $\mathbf{x}_j$ that maximizes dose to tumor, and minimizes dose to critical structures and body tissues for all $k \in \{1, \ldots, n\}$

$$\min \frac{1}{v_s} \sum_{s \in \text{OARs}} \|(b_s - \underline{w}_s \mathcal{D}_{ij}^s \mathbf{x}_s)_+\|_2^2 + \frac{1}{v_s} \sum_{s \in \text{PTVs}} \|(\bar{w}_s \mathcal{D}_{ij}^s \mathbf{x}_s - b_s)_+\|_2^2$$
$$\text{subject to } \mathbf{x} \geq 0.$$

- Restated as

$$\min \frac{1}{2}\|A\mathbf{x} - \mathbf{b}\|_2^2 \quad \text{subject to } x \geq 0.$$

FMO Lagrangian

- Lagrangian:

$$L(\mathbf{x}, \boldsymbol{\lambda}) = \frac{1}{2}\|A\mathbf{x} - \mathbf{b}\|_2^2 - \boldsymbol{\lambda}^T\mathbf{x}.$$

- Introduce the auxiliary variable $\mathbf{z}$, we have

$$\min_{\mathbf{x}} \frac{1}{2}\|\mathbf{A}\mathbf{x} - \mathbf{b}\|_2^2, \quad \text{subject to } \mathbf{z} = \mathbf{x}, \;\; \mathbf{z} \geq 0,$$

FMO Primal and Dual Updated

- Solving the $\mathbf{x}$ and $\mathbf{z}$ sub-problems, we have

$\mathbf{x}, \mathbf{z}$-updates

$$\mathbf{x}^{k+1} = \left(\mathbf{A}^T\mathbf{A} + \rho \boldsymbol{I}\right)^{-1}\left(\mathbf{A}^T\boldsymbol{b} + \rho \mathbf{z}^k - \boldsymbol{\lambda}^k\right)$$
$$\mathbf{z}^{k+1} = S_{\boldsymbol{\lambda}/\rho}\left(\mathbf{x}^{k+1} + \boldsymbol{\lambda}^k\right)$$

where $S_{\boldsymbol{\lambda}/\rho}(\tau) = (\mathbf{x} - \boldsymbol{\lambda}/\rho)_+ - (-\tau - \boldsymbol{\lambda}/\rho)_+$, and

$$\boldsymbol{\lambda}^{k+1} = \boldsymbol{\lambda}^k - \gamma(\mathbf{z}^{k+1} - \mathbf{x}^{k+1}),$$

with γ as the step length controlling parameter.

Results: Dose Wash Plot

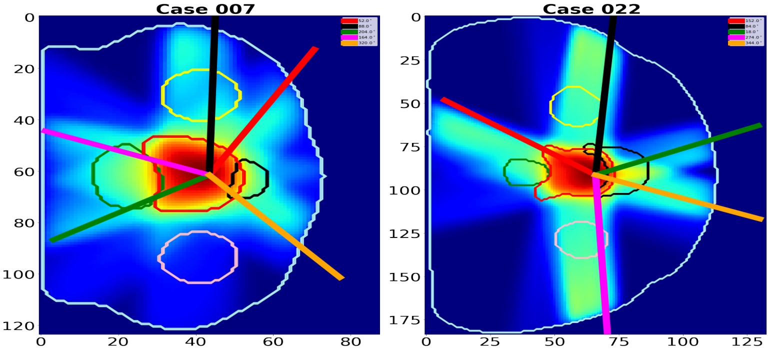

Results: Dose Wash

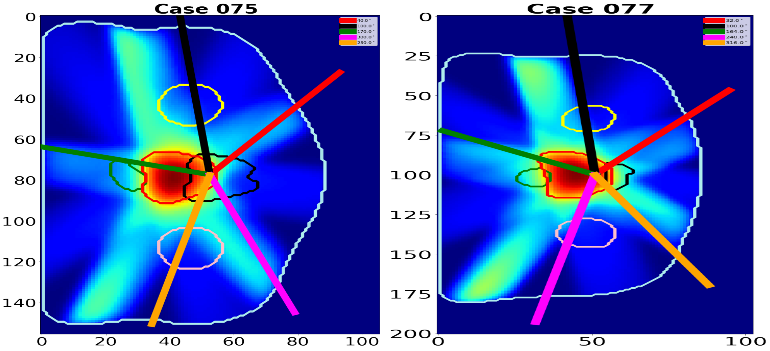

Previously Proposed Future Work (Last Fall)

- Supervised Pretraining
  - For example, PlanIQ or Column generation to eliminate plan quality gap and save training process time
  - Kalman filtering of predictions from neural network policy to obtain stable probabilities
- Robust policy improvement of pre-training angle predictions
  - e.g. Monte-Carlo Tree Search or Graph Convolutional Networks and guided tree search [Zhuwen et al. (2018)].

Supervised Pre-Training of Deep BOO Policy

This page is left blank intentionally.

Arthur L Boyer, Timothy G Ochran, Carl E Nyerick, Timothy J Waldron, and Calvin J Huntzinger. Clinical dosimetry for implementation of a multileaf collimator. *Medical physics*, 19(5):1255–1261, 1992. 4

Steve Webb. *Intensity-Modulated Radiation Therapy*. Institute of Physics Publishing Ltd, Bristol and Philadelphia, 2001. 4

Achim Schweikard, Rhea Tombropoulos, and John R Adler. Robotic Radiosurgery with Beams of Adaptable Shapes. In Nicholas Ayache, editor, *Computer Vision, Virtual Reality and Robotics in Medicine*, pages 138–149, Berlin, Heidelberg, 1995. Springer Berlin Heidelberg. ISBN 978-3-540-49197-2. 6

Steve Webb. Conformal intensity-modulated radiotherapy (imrt) delivered by robotic linac-testing imrt to the limit? *Physics in Medicine & Biology*, 44(7):1639, 1999. 6

Rodney D Wiersma, Zhifei Wen, Meredith Sadinski, Karl Farrey, and Kamil M Yenice. Development of a frameless stereotactic radiosurgery system based on real-time 6d position monitoring and adaptive head motion compensation. *Physics in Medicine & Biology*, 55(2):389, 2009. 7

Christian Herrmann, Lei Ma, and Klaus Schilling. Model Predictive Control For Tumor Motion Compensation In Robot Assisted Radiotherapy. *IFAC Proceedings Volumes*, 44(1):5968–5973, 2011. 8

Olalekan Ogunmolu, Adwait Kulkarni, Yonas Tadesse, Xuejun Gu, Steve Jiang, and Nicholas Gans. Soft-neuroadapt: A 3-dof neuro-adaptive patient pose correction system for frameless and maskless cancer radiotherapy. In *IEEE/RSJ International Conference on Intelligent Robots and Systems (IROS), Vancouver, BC, CA*, pages 3661–3668. IEEE, 2017. 26

Matthieu Nesme, Maud Marchal, Emmanuel Promayon, Matthieu Chabanas, Yohan Payan, and François Faure. Physically Realistic Interactive Simulation For Biological Soft Tissues. *Recent Research Developments in Biomechanics*, 2:1–22, 2005. 32

Matthieu Nesme, François Faure, and Yohan Payan. Hierarchical Multi-Resolution Finite Element Model for Soft Body Simulation. *Lecture Notes in Computer Science*, 4072:40–47, 2006. 32

James M Bern, Grace Kumagai, and Stelian Coros. Fabrication, modeling, and control of plush robots. In *Intelligent Robots and Systems (IROS), 2017 IEEE/RSJ International Conference on*, pages 3739–3746. IEEE, 2017. 32

Alan Gent. *Engineering with Rubber. How to Design Rubber Components*. Carl Hanser Verlag Publicationbs, Munich, 2012. 32

Michael W Hannan and Ian D Walker. Kinematics and the Implementation of an Elephant's Trunk Manipulator and Other Continuum Style Robots. *Journal of Robotic Systems*, 20(2):45–63, 2003. 32

Michael W Hannan and Ian D. Walker. Novel Kinematics for Continuum Robots. pages 227–238. Advances in Robot Kinematics, 2000. 32

Bryan A Jones and Ian D Walker. Kinematics for Multisection Continuum Robots.pdf. 22(1):43–55, 2006. 32

Federico Renda, Michele Giorelli, Marcello Calisti, Matteo Cianchetti, and Cecilia Laschi. Dynamic model of a multibending soft robot arm driven by cables. *IEEE Transactions on Robotics*, 30(5):1109–1122, 2014. 32

Deepak Trivedi, Amir Lotfi, and Christopher D Rahn. Geometrically Exact Models For Soft Robotic Manipulators. *IEEE Transactions on Robotics*, 24(4):773–780, 2008. 32

Hiromi Mochiyama. Hyper-flexible robotic manipulators. In *IEEE International Symposium on Micro-NanoMechatronics and Human Science, 2005*, pages 41–46. IEEE, 2005. 32

Gregory S Chirikjian and Joel W Burdick. The kinematics of hyper-redundant robot locomotion. *IEEE transactions on robotics and automation*, 11(6):781–793, 1995. 32

Gregory S Chirikjian. Hyper-redundant manipulator dynamics: A continuum approximation. *Advanced Robotics*, 9(3):217–243, 1994. 32

Yoram Yekutieli, Roni Sagiv-Zohar, Ranit Aharonov, Yaakov Engel, Binyamin Hochner, and Tamar Flash. A dynamic model of the octopus arm. i. biomechanics of the octopus reaching movement. *Journal of neurophysiology*, 2005. 32

Tianjiang Zheng, David T Branson, Rongjie Kang, Matteo Cianchetti, Emanuele Guglielmino, Maurizio Follador, Gustavo A Medrano-Cerda, Isuru S Godage, and Darwin G Caldwell. Dynamic continuum arm model for use with underwater robotic manipulators inspired by octopus vulgaris. In *2012 IEEE International Conference on Robotics and Automation*, pages 5289–5294. IEEE, 2012. 32

Frédéric Boyer, Mathieu Porez, and Wisama Khalil. Macro-continuous computed torque algorithm for a three-dimensional eel-like robot. *IEEE Transactions on Robotics*, 22(4):763–775, 2006. 32

R.W. Ogden. *Non-linear Elastic Deformations*. Dover Publicationbs, Inc., Mineola, New York, 1997. 32

Audrey Sedal, Daniel Bruder, Joshua Bishop-Moser, Ram Vasudevan, and Sridhar Kota. A continuum model for fiber-reinforced soft robot actuators. *Journal of Mechanisms and Robotics*, 10(2):024501, 2018. 32

Gerhard A Holzapfel, Thomas C Gasser, and Ray W Ogden. A new constitutive framework for arterial wall mechanics and a comparative study of material models. *Journal of elasticity and the physical science of solids*, 61(1-3):1–48, 2000. 32

D Caleb Rucker, Bryan A Jones, and Robert J Webster III. A geometrically exact model for externally loaded concentric-tube continuum robots. *IEEE transactions on robotics: a publication of the IEEE Robotics and Automation Society*, 26(5):769, 2010. 32

Hasan Demirkoparan and Thomas J Pence. Swelling of an Internally Pressurized Nonlinearly Elastic Tube with Fiber Reinforcing. *International journal of solids and structures*, 44(11-12):4009–4029, 2007. 32

Van-Duc Nguyen. Constructing force-closure grasps. *The International Journal of Robotics Research*, 7(3): 3–16, 1988. 54

Olalekan Patrick Ogunmolu. *A Multi-DOF Soft Robot Mechanism for Patient Motion Correction and Beam Orientation Selection in Cancer Radiation Therapy*. PhD thesis, The University of Texas at Dallas, 2019. 57, 61

Thomas Bortfeld and Wolfgang Schlegel. Optimization of beam orientations in radiation therapy: Some theoretical considerations. *Physics in Medicine & Biology*, 38(2):291, 1993. 73

Svante Södertröm and Anders Brahme. Optimization of the Dose Delivery In A Few Field Techniques Using Radiobiological Objective Functions. *Medical physics*, 20(4):1201–1210, 1993. 73

AB Pugachev, AL Boyer, and L Xing. Beam orientation optimization in intensity-modulated radiation treatment planning. *Medical Physics*, 27(6):1238–1245, 2000. 73

Andrei Pugachev and Lei Xing. Incorporating prior knowledge into beam orientaton optimization in imrt. *International Journal of Radiation Oncology* Biology* Physics*, 54(5):1565–1574, 2002. 73

Dionne M Aleman, Arvind Kumar, Ravindra K Ahuja, H Edwin Romeijn, and James F Dempsey. Neighborhood Search Approaches to Beam Orientation Optimization i Intensity Modulated Radiation Therapy Treatment Planning. *Journal of Global Optimization*, 42(4):587–607, 2008. 73

Dimitris Bertsimas, Valentina Cacchiani, David Craft, and Omid Nohadani. A Hybrid Approach To Beam Angle Optimization In Intensity-modulated Radiation Therapy. *Computers & Operations Research*, 40 (9):2187–2197, 2013. 73

Jörg Stein, Radhe Mohan, Xiao-Hong Wang, Thomas Bortfeld, Qiuwen Wu, Konrad Preiser, C Clifton Ling, and Wolfgang Schlegel. Number and orientations of beams in intensity-modulated radiation treatments. *Medical Physics*, 24(2):149–160, 1997. 73

David Craft. Local beam angle optimization with linear programming and gradient search. *Physics in Medicine & Biology*, 52(7):N127, 2007. 73

Renzhi Lu, Richard J Radke, Linda Hong, Chen-Shou Chui, Jianping Xiong, Ellen Yorke, and Andrew Jackson. Learning The Relationship Between Patient Geometry And Beam Intensity In Breast Intensity-modulated Radiotherapy. *IEEE transactions on biomedical engineering*, 53(5):908–920, 2006. 73

Yongjie Li and Jie Lei. A Feasible Solution To The Beam-angle-optimization Problem In Radiotherapy Planning With A Dna-based Genetic Algorithm. *IEEE Transactions on biomedical engineering*, 57(3): 499–508, 2010. 73

Chuang Wang, Jianrong Dai, and Yimin Hu. Optimization Of Beam Orientations And Beam Weights For Conformal Radiotherapy Using Mixed Integer Programming. *Physics in Medicine & Biology*, 48(24): 4065, 2003. 73

Warren D D'Souza, Robert R Meyer, and Leyuan Shi. Selection Of Beam Orientations In Intensity-modulated Radiation Therapy Using Single-beam Indices And Integer Programming. *Physics in Medicine & Biology*, 49(15):3465, 2004. 73

Gino J Lim, Michael C Ferris, Stephen J Wright, David M Shepard, and Matthew A Earl. An optimization framework for conformal radiation treatment planning. *INFORMS Journal on Computing*, 19(3): 366–380, 2007. 73

Xun Jia, Chunhua Men, Yifei Lou, and Steve B. Jiang. Beam Orientation Optimization For Intensity Modulated Radiation Therapy Using Adaptive L2,1-minimization. *Physics in Medicine and Biology*, 56 (19):6205–6222, 2011. 73

Johannes Heinrich, Marc Lanctot, and David Silver. Fictitious self-play in extensive-form games. In *International Conference on Machine Learning*, pages 805–813, 2015. 74

Li Zhuwen, Qifeng Chen, and Vladlen Koltun. Combinatorial optimization with graph convolutional networks and guided tree search. In *Advances in Neural Information Processing Systems*. NeurIPS, 2018. 85

Azar Sadeghnejad Barkousaraie, Olalekan Ogunmolu, Dan Nguyen, and Steve Jiang. Using Supervised Learning and Guided Monte Carlo Tree Search for Beam Orientation Optimization in Radiation Therapy. In *Under Review at International Conference on Medical Image Computing and Computer Assisted Intervention, XXII*, 2019a. 87

Azar Sadeghnejad Barkousaraie, Olalekan Ogunmolu, Steve Jiang, and Dan Nguyen. A Fast Deep Learning Approach for Beam Orientation Selection Using Supervised Learning with Column Generation on IMRT Prostate Cancer Patients. *Medical Physics, American Association of Physicists in Medicine*, 2019b. 87